
AN OPTIMIZATION FRAMEWORK FOR WIND FARM LAYOUT DESIGN USING CFD-BASED KRIGING MODEL

A PREPRINT

Zhenfan Wang

School of Naval Architecture, Ocean and Civil Engineering
Shanghai Jiao Tong University
Shanghai 200240, China
sjtu-wzf@sjtu.edu.cn

Yu Tu

School of Naval Architecture, Ocean and Civil Engineering
Shanghai Jiao Tong University
Shanghai 200240, China

Kai Zhang

School of Naval Architecture, Ocean and Civil Engineering
Shanghai Jiao Tong University
Shanghai 200240, China
kai.zhang@sjtu.edu.cn

Zhaolong Han

School of Naval Architecture, Ocean and Civil Engineering, Shanghai Jiao Tong University
Shanghai 200240, China

Yong Cao

School of Naval Architecture, Ocean and Civil Engineering, Shanghai Jiao Tong University
Shanghai 200240, China

Dai Zhou

School of Naval Architecture, Ocean and Civil Engineering, Shanghai Jiao Tong University
Shanghai 200240, China

August 28, 2023

ABSTRACT

Wind farm layout optimization (WFLO) seeks to alleviate the wake loss and maximize wind farm power output efficiency, and is a crucial process in the design and planning of wind energy projects. Since the optimization algorithms typically require thousands of numerical evaluations of the wake effects, conventional WFLO studies are usually carried out with the low-fidelity analytical wake models, while the higher-fidelity computational-fluid-dynamics-based (CFD-based) methods are seldom used due to the excessive computational cost. In this paper, we develop a self-adaptive optimization framework for wind farm layout design using CFD-based Kriging model to maximize the annual energy production (AEP) of wind farms. This surrogate-based optimization (SBO) framework uses latin hypercube sampling to generate a group of wind farm layout samples, based on which CFD simulations with the turbines modeled as actuator disks are carried out to obtain

the corresponding AEPs. This initial wind farm layout dataset is used to train the Kriging model, which is then integrated with an optimizer based on genetic algorithm (GA). As the optimization progresses, the intermediate optimal layout designs are again fed into the dataset to re-train the Kriging model. Such adaptive update of wind farm layout dataset continues until the algorithm converges to the optimal layout design. To evaluate the performance of the proposed SBO framework, we apply it to three wind farm cases under different wind distribution and terrains. Compared to the conventional staggered layout along the dominant wind direction, the optimized wind farm produces significantly higher total AEP, which is more evenly distributed among the turbines. In particular, the SBO framework requires significantly smaller number of CFD calls to yield the optimal layouts that generates almost the same AEP with the direct CFD-GA method. Further analysis on the velocity fields show that the optimization framework always attempts to locate the downstream turbines away from the wakes of upstream ones along the dominant wind directions. The proposed CFD-based surrogate model provides a more accurate and flexible alternative to the conventional analytical-wake-model-based methods in WFLO tasks, and has the potential to be used for designing efficient wind farm projects.

Keywords Wind farm layout design · Surrogate-based optimization · Kriging model · Actuator disk model

1 Introduction

An increasing number of countries have committed to developing sustainable energy as substitutes for fossil fuels due to pressing environmental issues. As wind energy is one of the most economically competitive and abundant renewable energy, wind farms have been installed worldwide to harvest this clean energy resources. However, the interaction between turbines within wind farms, particularly the wake effects generated by upstream turbines, can have a substantial impact on the performance of downstream turbines. These wake effects lead to lower wind speeds and increased turbulence intensity, resulting in reduced power generation. It is reported that the average power loss reaches 10% – 20% in some large offshore wind farms due to the wake effects [Barthelmie et al., 2009].

As an effective means to alleviate the wake effects within wind farms at the initial designing phase, wind farm layout optimization (WFLO) has been a subject of extensive researches [Reddy, 2020, Dong et al., 2021, Thomas et al., 2022a]. Table 1 presents a selective summary of the existing studies on WFLO in terms of the optimization algorithm and the wake model. Both the gradient-based methods such as sparse nonlinear optimizer (SNOPT) and Sequential Convex Programming (SCP), and the heuristic search techniques such as the greedy algorithm, genetic algorithm (GA), particle swarm optimization algorithm (PSO), ant colony optimization (ACO), have been applied in these studies. Two main types of wake models are used in WFLO, namely the analytical wake models and the numerical wake models.

Analytical wake models such as the Jensen wake model [Jensen, 1983], the Gaussian model [Larsen, 1988], the Frandsen wake model [Frandsen et al., 2006] are most widely applied in WFLO problems due to the high computational efficiency. These models employ simplified analytical functions based on momentum conservation or empirical relations to describe the turbine’s wake characteristics. The most used Jensen model assumes that the wake expands linearly, and the velocity deficit is determined by the distance behind the turbine, wind speed and induction parameter. The Gaussian wake model assumes that the velocity deficit follows a Gaussian distribution. It provides a more realistic representation of the wake’s shape compared to the linear wake expansion in Jensen’s model. The Frandsen wake model incorporates both linear and Gaussian wake expansions, and offers more accurate predictions by accounting for the initial wake width. Although these analytical models provide valuable insights into the wake development behind wind turbines, they are simplifications of the complex physics involved in wake interactions, and can be less accurate in assessing the wake effects.

Numerical simulations based on computational fluid dynamics (CFD) presents a higher-fidelity method for understanding the aerodynamics of wind turbines. Depending on the way the turbines are modeled, the CFD-based methods can be classified as blade-resolved simulation, actuator line model, and actuator disk model. Blade-resolved simulations provide detailed insights into the flow characteristics around individual blades, including the effects of turbulence, separation, and dynamic stall [Mittal et al., 2016, Liu et al., 2017, de Oliveira et al., 2022, Zhang et al., 2023]. However, the huge computational resources required for resolving the blade boundary layer preclude its use for large-scale wind farm studies. The actuator line model (ALM) treats the rotor blades as lines distributed with actuator points, on which the sectional drag and lift forces are projected. Since these aerodynamic forces are calculated based on tabulated airfoil data, this approach removes the computational complexity associated with resolving the rotor blades. ALM has been regarded as the state-of-the-art tool for wind farm simulations [Stevens and Meneveau, 2017, Stevens et al., 2018, Shapiro et al., 2022]. Nevertheless, in the case of WFLO where iterative evaluations of the velocity deficit are required, ALM is still prohibitively expensive.

Table 1: A review of the wind farm layout optimization studies

| Reference | Optimization algorithms | Wake models |
|--------------------------------------|-------------------------|-------------------|
| Mosetti et al. [1994] | GA | Jensen |
| Ozturk and Norman [2004] | Greedy | - |
| Grady et al. [2005] | GA | Jensen |
| Mora et al. [2007] | GA | Jensen |
| Zhang et al. [2011] | Greedy | Jensen |
| Eroğlu and Seçkiner [2012] | ACO | Jensen |
| Chen et al. [2013] | GA | Frandsen |
| Park and Law [2015] | SCP | Jensen |
| Shakoor et al. [2015] | GA | Jensen |
| Hou et al. [2016] | PSO | Jensen |
| Gebraad et al. [2017] | SNOPT | Floris wake model |
| Parada et al. [2017] | GA | BP |
| Pillai et al. [2017] | GA & PSO | Larsen |
| Kirchner-Bossi and Porté-Agel [2018] | GA | Gaussian |
| Stanley and Ning [2019] | SNOPT | Gaussian |
| Quan and Kim [2019] | Greedy | Jensen |
| Cruz and Carmo [2020] | GA | CFD-ADM |
| Antonini et al. [2020] | SQP | CFD-ADM |
| Stanley et al. [2020] | SNOPT | BP |
| Gagakuma et al. [2021] | SNOPT | Floris wake model |
| Liu et al. [2021] | GA | Ishihara |
| Thomas et al. [2022b] | SNOPT & ALPSO | Gaussian |

Another popular method in the actuator-type modeling technique is the actuator disk model (ADM). This model further simplifies the rotor swept area as permeable disk. The thrust and torque of the rotor are added to the actuator zone as source terms, which generate pressure drops and velocity plunges across the disk area in the CFD simulations [Sanderse et al., 2011, Svenning, 2010]. Compared with ALM, the more intricate flow structures such as root and tip vortices can not be captured by ADM. Nevertheless, the ADM has been shown to depict wake effects with sufficient accuracy [Martínez-Tossas et al., 2015]. In recent years, CFD simulations with ADM has been applied in WFLO problems. Antonini et al. [2020] presented a gradient-based algorithm with adjoint method for gradient calculation to solve the optimization of wind farm layout using ADM. The authors claimed that this CFD-based method is able to accurately simulate wake effects and terrain-induced flow characteristics. Cruz and Carmo [2020] applied the heuristic genetic algorithm to optimize the layout of wind farm with terrain effects using CFD. While the authors also commended the superior accuracy of ADM over the analytical wake model in WFLO tasks, they noted that significant amount of computational resources are required for the optimization algorithm to converge to the optimal layout design.

To alleviate the computational challenges of using high-fidelity CFD-based methods in WFLO problems, we propose to apply the Kriging model as a surrogate to accelerate the optimization process. The Kriging model, also known as Gaussian Process Regression (GPR), was initially developed as a geostatistical method for spatial interpolation and prediction of correlated data [Kriging, 1951]. It estimates the unknown values at unobserved locations by taking into account the observed values at nearby locations and their spatial relationships. Once this surrogate model is trained, the wake effects and the energy production of a particular layout can be obtained at a low computational cost and without the need of new CFD simulations. The applicability of Kriging model has been demonstrated in various disciplines such as image segmentation [Karl, 2010], hull shape optimization [Casella, 2020], aero-elastic tailoring of bridge decks [Montoya et al., 2022], just to name a few. However, the feasibility of using Kriging model for high-fidelity wind farm design has not been reported before.

In this paper, we develop a self-adaptive optimization framework for high-fidelity wind farm layout design using surrogate-based optimization (SBO) method. Using this framework, we optimize the siting of each turbine within a restricted area to maximize wind farm’s annual energy production (AEP) with reduced computational cost. The rest of the paper is organized as follows: Section 2 outlines the formulation of the WFLO problems and the self-adaptive WFLO framework, including the wind farm layout dataset, the numerical method, and the surrogate-based optimization (SBO) method using Kriging. In Section 3, we present three wind farm cases under different wind distributions and terrains to demonstrate the performance and advantages of our proposed framework. Finally, Section 4 presents the conclusions and potential future research directions.

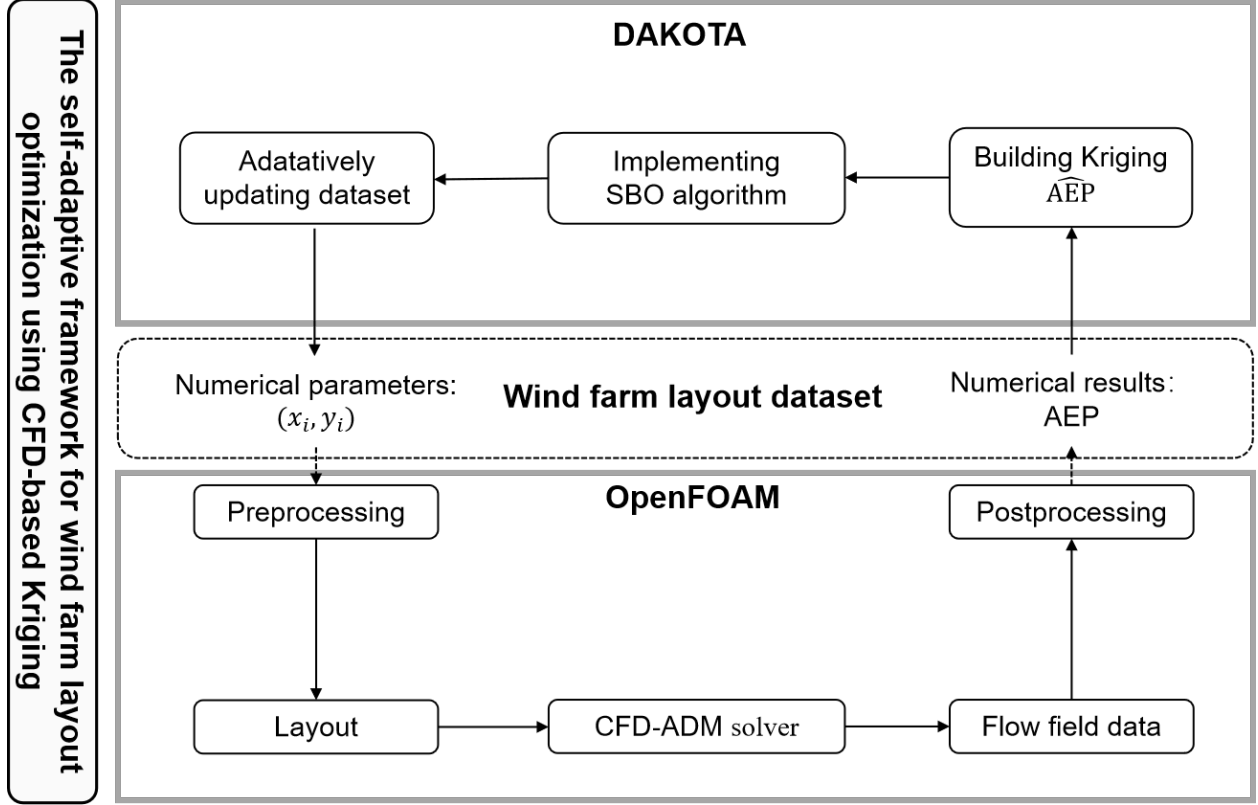


Figure 1: Flow chart of the self-adaptive WFLO framework.

2 Self-adaptive WFLO framework

In this section, we present the details about the proposed wind farm layout optimization (WFLO) framework. The formulation of the WFLO problem is formally introduced in §2.1. Next, we outline the three main procedures involved in the framework, i.e., the adaptive wind farm layout dataset (§2.2), the prediction of AEP using CFD simulations (§2.3), and the construction of Kriging model for surrogate-based optimization (§2.4). Figure 1 illustrates the self-adaptive WFLO framework. The open-source CFD toolbox OpenFOAM is used for wind farm CFD simulations and AEP prediction. The construction of Kriging model and implementation of SBO are carried out using optimization toolbox DAKOTA. Python and shell glue scripts are created to couple these toolboxes.

2.1 Formulation of WFLO problem

The objective of the WFLO problem is to find the optimal location of each wind turbine to maximize annual energy production (AEP) of the wind farm:

$$\text{AEP} = \frac{365 \times 3 + 366}{4} \times 24 \sum_{i=1}^n \sum_{j=1}^m P_j(x_i, y_i) f_j,$$

where n, m denote numbers of turbine and wind directions respectively, P_j is turbine's power output under wind direction j , f_j is the frequency of wind direction j . (x_i, y_i) is the coordinate of turbine i , and is the design variable in this study. To reduce computational cost, we choose to solve a discrete optimization problem by splitting the siting area into square cells as candidate positions for wind turbines [Bai et al., 2022]. It was shown in Thomas et al. [2022a] that the limitation on potential turbine locations does not necessarily preclude such methods from finding optimal layouts. In WFLO problem, additional inter-distance requirement is defined as:

$$\text{subject to } d_i \geq d_{min},$$

where d_i is the inter-distance between turbines, and must be greater than or equal to $d_{min} = 2D$.

2.2 Adaptive wind farm layout dataset

The wind farm layout parameters and the corresponding AEP acquired from CFD simulations form the wind farm layout dataset. It is comprised of two groups of data, the initial sampling data and iteratively updated data. The distribution of initial samples determines the performance of the framework. Therefore, it needs to be equally distributed throughout design space. We use latin hypercube sampling (LHS) method [McKay et al., 2000] to produce the initial samples of layout parameters, $\mathbf{X} = \{\mathbf{x}^{(1)}, \mathbf{x}^{(2)}, \dots, \mathbf{x}^{(n)}\}^T$. The $\mathbf{x}^{(i)} = \{(x_1^{(i)}, y_1^{(i)}), (x_2^{(i)}, y_2^{(i)}), \dots, (x_k^{(i)}, y_k^{(i)})\}$ represents turbines' horizontal coordinate set in the i th sample of layout. CFD simulations are carried out based on the layout parameters, and the annual energy production (AEP) is collected in $\mathbf{Y} = \{\text{AEP}^{(1)}, \text{AEP}^{(2)}, \dots, \text{AEP}^{(n)}\}^T$. The iterative update of dataset is explained in section 2.4.

2.3 Wind farm CFD simulations

In this study, CFD simulations are carried out to model the wake interactions with the rotors treated as actuator disks. The power production of each turbine is predicted using the the ADM-RANS simulations, as illustrated below.

2.3.1 Governing equations

We numerically solve for the flows over the wind turbines by employing Reynolds-averaged Navier-Stokes (RANS) formulation

$$\frac{\partial \bar{u}_i}{\partial x_i} = 0, \quad (1a)$$

$$\rho \frac{\partial \bar{u}_i}{\partial t} + \rho \frac{\partial (\bar{u}_i \bar{u}_j)}{\partial x_j} = -\frac{\partial \bar{p}}{\partial x_i} + \frac{\partial}{\partial x_j} \left(\mu \left(\frac{\partial \bar{u}_i}{\partial x_j} + \frac{\partial \bar{u}_j}{\partial x_i} \right) - \overline{\rho u'_j u'_i} \right) + f_i, \quad (1b)$$

where x_i is Cartesian space coordinate, \bar{u}_i and \bar{p} are the temporally averaged velocity and pressure, respectively. ρ and μ are the air density and dynamic viscosity, f_i represents the source term from the actuator disk. The Reynolds stress emerged from the time-average process $\overline{\rho u'_j u'_i}$ is modeled using the $k - \epsilon$ turbulence model with the introduction of two new variables, i.e., the turbulence kinematic energy k , and the dissipation rate ϵ . The standard transport equations for the two new variables read as

$$\rho \frac{\partial k}{\partial t} + \rho \frac{\partial (\bar{u}_i k)}{\partial x_i} = \frac{\partial}{\partial x_j} \left(\frac{\mu_t}{\sigma_k} \frac{\partial k}{\partial x_j} \right) + P_k - \rho \epsilon, \quad (2a)$$

$$\rho \frac{\partial \epsilon}{\partial t} + \rho \frac{\partial (\bar{u}_i \epsilon)}{\partial x_i} = \frac{\partial}{\partial x_j} \left(\frac{\mu_t}{\sigma_\epsilon} \frac{\partial \epsilon}{\partial x_j} \right) + C_{1\epsilon} \frac{\epsilon}{k} P_k - C_{2\epsilon} \frac{\epsilon^2}{k} \rho, \quad (2b)$$

with

$$P_k = -\overline{\rho u'_j u'_i} \frac{\partial u_j}{\partial x_i}, \quad (3a)$$

$$\mu_t = -\rho C_\mu \frac{k^2}{\epsilon}, \quad (3b)$$

where C_μ , σ_k , σ_ϵ , $C_{1\epsilon}$, $C_{2\epsilon}$ are the five constants in the $k - \epsilon$ turbulence model and are set as default values in OpenFOAM.

The RANS equations outlined above are discretized using the finite volume method with second-order numerical schemes in both space and time. A modified version of the simpleFoam solver (OpenFOAM package) is used for solving for the steady-state flow over the wind turbines. The modification involves adding the ADM source term into the RANS equations, as we discuss in detail next.

2.3.2 Actuator disk model

The actuator disk model (ADM) simulates the turbine rotor as a thin, permeable disk, and the momentum transferred from rotor to the flow is added to the flow as volumetric source term f_i , as mentioned in equation 1. To implement wind farm CFD simulations, thrust and torque of each rotor are required. Ideally, these aerodynamic quantities can be obtained by looking up the thrust and torque curves provided by wind turbine manufacturers, given the theoretical inflow velocity. However, in the presence of the wake effects within wind farm, the theoretical inflow velocity for the downstream turbine is not known *a priori*.

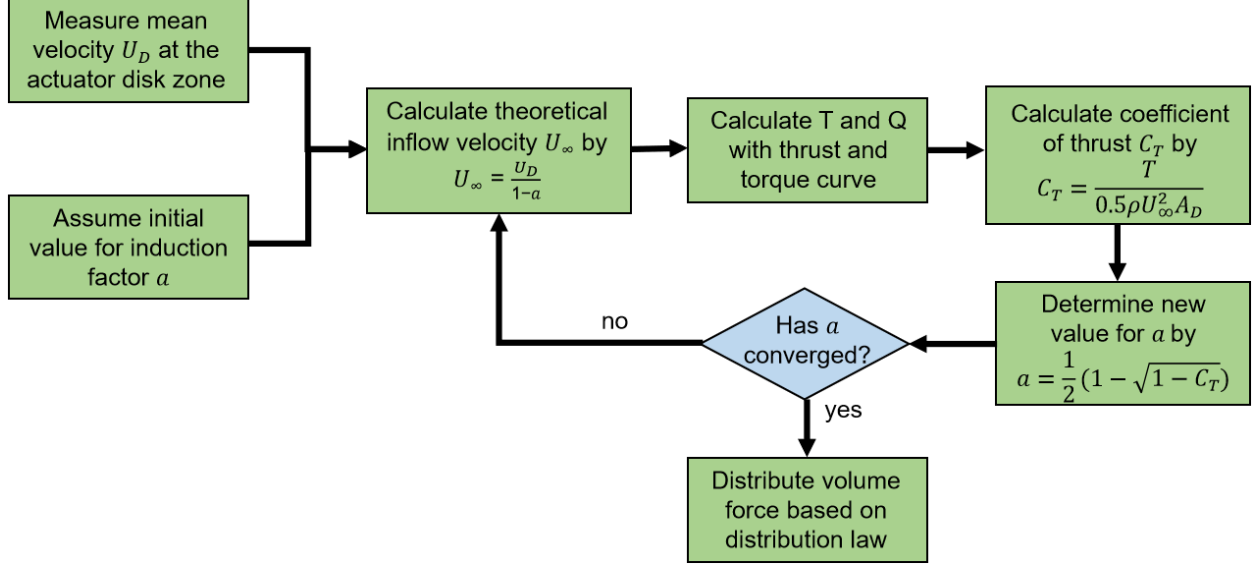


Figure 2: Workflow to calculate inflow velocity, thrust and torque in the ADM code

To circumvent this problem, we follow the approach in Richmond et al. [2019], where the thrust and torque curves are inserted into the flow solver, and the theoretical inflow velocity is calculated in an iterative manner. This method, which is summarized in figure 2, is based on the one-dimensional actuator disk theory [Burton et al., 2011]:

$$U_D = U_\infty(1 - a), \quad (4a)$$

$$C_T = \frac{T}{\frac{1}{2}\rho U_\infty^2 A_D}, \quad (4b)$$

$$C_T = 4a(1 - a), \quad (4c)$$

$$a = \frac{1}{2}(1 - \sqrt{1 - C_T}), \quad (4d)$$

where U_D is the velocity averaged over the disk region, C_T is the coefficient of thrust, A_D is the area of actuator disk, and a is axial induction factor. This equation is solved iteratively within the modified simpleFoam code, for each turbine at each solver iteration, until the convergence criteria is met.

After the thrust and torque of each rotor are obtained, the volume forces are distributed along the radial direction following the Goldstein optimum [Goldstein, 1929]:

$$f_{ix} = A_x r^* \sqrt{1 - r^*}, \quad (5a)$$

$$f_{i\theta} = A_\theta \frac{r^* \sqrt{1 - r^*}}{r^*(1 - r'_h) + r'_h}, \quad (5b)$$

with

$$r^* = \frac{r' - r'_h}{1 - r'_h}, \quad r' = \frac{r}{R_P}, \quad (6a)$$

$$A_x = \frac{105}{8} \frac{T}{\pi \Delta (3R_H + 4R_P)(R_P - R_H)}, \quad (6b)$$

$$A_\theta = \frac{105}{8} \frac{Q}{\pi \Delta R_P (3R_P + 4R_H)(R_P - R_H)}, \quad (6c)$$

where f_{ix} is axial force, $f_{i\theta}$ is tangential force, r is the distance between the point and disk center, R_P is the external radius of disk, R_H is the internal radius of disk, T is rotor's thrust, Q is rotor's torque, and Δ is the thickness of disk.

Finally, the objective function, AEP, is predicted by the sum of power of each individual cell within actuator disk zones as

$$P = \sum_{i=1}^k P_i = \sum_{i=1}^k F_i U_i \quad (7)$$

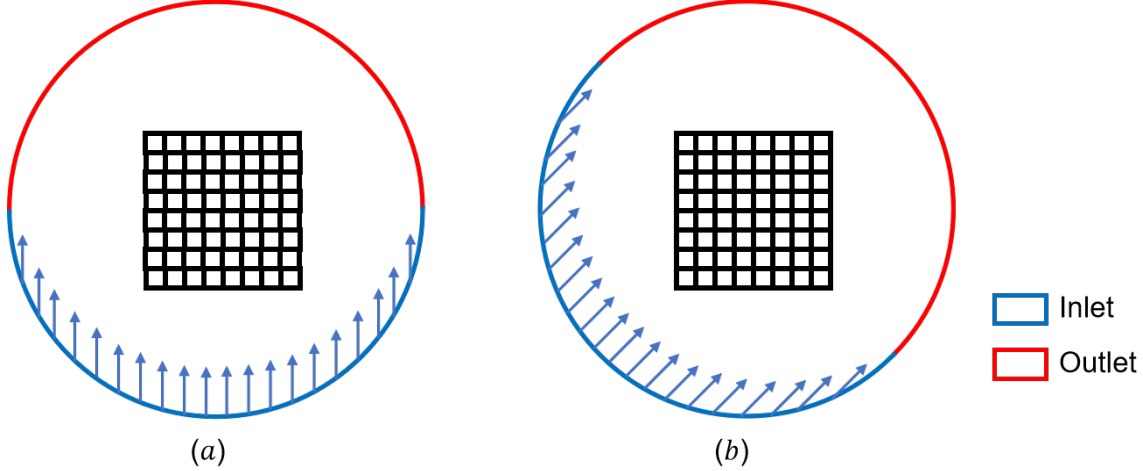


Figure 3: Top views of the circular computational domain for a wind farm. (a) assigning inlet or outlet boundary for wind direction of 180° , (b) assigning inlet or outlet boundary for wind direction of 225° .

where F_i and U_i are vectors of volume force and velocity in each individual cell, and k is total number of cells in the disk zone.

2.3.3 Computational setup

We adopt a circular computational domain that allows for simulations with different inflow directions, as illustrated in figure 3. The wind turbines are restricted within a rectangular subdomain in the center. The diameter of the circular computational domain is set as 3 times the length of the center rectangle. In the vertical direction, the height of the computational domain is set as $8D$, where D is the diameter of the rotor. The inlet velocity is prescribed as $U_{in} = U_\infty(z/z_0)^\alpha$, where z_0 is the height of the turbine hub, $U_\infty = 11.4$ m/s is the reference velocity at the turbine hub, and $\alpha = 0.14$ is the shear rate of the velocity profile. At the outlet, a reference pressure $p_\infty = 0$ is set, with zero gradient condition for the velocity. The bottom side of the computational domain is treated as wall, and the top boundary as slip condition.

The mesh of the computational domain is created using OpenFOAM's native blockMesh tool. To guarantee that ADM's source terms are loaded into the flow, meshes near actuator disk zone are refined. The element size in disk region is 6 m ($0.05D$). For a simulation with 8 turbines, the total number of control volumes is around $2 \times 10^5 - 6 \times 10^5$.

2.4 Surrogate-based optimization method

2.4.1 Kriging model

The Kriging model [Krige, 1951] is employed in this framework to build the surrogate model. It predicts the response values at unknown points based on a set of sample input data $\mathbf{X} = \{\mathbf{x}^{(1)}, \mathbf{x}^{(2)}, \dots, \mathbf{x}^{(n)}\}^T$, and the observed values $\mathbf{Y} = \{y^{(1)}, y^{(2)}, \dots, y^{(n)}\}^T$.

The Kriging emulator, $\hat{f}(x)$, is defined in the following equation [Dalbey et al., 2022, Adams et al., 2020]:

$$\hat{f}(\mathbf{x}) = g(\mathbf{x})^T \beta + \epsilon(\mathbf{x}), \quad (8)$$

where $\hat{\cdot}$ denotes the Kriging approximation, \mathbf{x} is the vector with all the design variables, $g(\mathbf{x})\beta$ is the vector of trend functions, $\epsilon(\mathbf{x})$ is Gaussian process error model which has zero uncertainty at the training points. The covariance matrix $\epsilon(\mathbf{x})$ is modeled using the correlation matrix as

$$\text{Cov}[\epsilon(\mathbf{x}^{(i)}), \epsilon(\mathbf{x}^{(j)})] = \sigma^2 r(\mathbf{x}^{(i)}, \mathbf{x}^{(j)}), \quad (9)$$

where $r(\mathbf{x}^{(i)}, \mathbf{x}^{(j)})$ is the correlation functions between samples $\mathbf{x}^{(i)}$ and $\mathbf{x}^{(j)}$.

In this framework, the Gaussian correlation function is used to calculate the correlation vector and matrix. The correlation vector and matrix are constructed by the following equations:

$$r(\mathbf{x}^{(i)}, \mathbf{x}^{(j)}) = \exp\left(-\sum_{k=1}^m \theta_k |x_k^{(i)} - x_k^{(j)}|^2\right), \quad i, j = 1, 2, \dots, n \quad (10a)$$

$$\mathbf{R} = \begin{pmatrix} r(\mathbf{x}^{(1)}, \mathbf{x}^{(1)}) & \dots & r(\mathbf{x}^{(1)}, \mathbf{x}^{(n)}) \\ \vdots & \ddots & \vdots \\ r(\mathbf{x}^{(n)}, \mathbf{x}^{(1)}) & \dots & r(\mathbf{x}^{(n)}, \mathbf{x}^{(n)}) \end{pmatrix}, \quad (10b)$$

where m is the number of dimensions in the search space; n is number of samples; θ is hyperparameter that affects correlations between samples.

The hyperparameters θ is estimated via Maximum Likelihood Estimation (MLE) method. To simplify MLE, the natural logarithm is used and constant terms are omitted:

$$\ln(L) = -\frac{n}{2} \ln|\mathbf{R}| - \frac{1}{2} \ln(\hat{\sigma}^2), \quad (11)$$

where $\hat{\sigma}^2 = (\mathbf{Y} - \mathbf{G}\beta)^T \mathbf{R}^{-1} (\mathbf{Y} - \mathbf{G}\beta) / n$ is the MLE of σ^2 and \mathbf{G} is an $n \times q$ matrix with rows $\mathbf{g}(\mathbf{x})_i^T$ (the trend function evaluated at point i). Maximizing the equation (11), we obtain the MLE of hyperparameter θ which in turn determines $\hat{\sigma}^2$.

When MLE is done, we obtain the Kriging emulator of unknown truth function. The predicted value $\hat{f}(\mathbf{x})$ at a new point \mathbf{x} is:

$$\hat{f}(\mathbf{x}) = \mathbf{g}(\mathbf{x})^T \beta + \mathbf{r}(\mathbf{x})^T \mathbf{R}^{-1} (\mathbf{Y} - \mathbf{G}\beta), \quad (12)$$

where $\mathbf{r}(\mathbf{x})$ is the vector of correlation between \mathbf{x} and each of training points.

Based on the wind farm layout dataset, a high-fidelity Kriging model $\widehat{\text{AEP}}(x_1, y_1, x_2, y_2, \dots, x_n, y_n)$ for wind farm AEP prediction is built with the aforementioned process and coupled to optimization algorithms. The adaptive SBO method is introduced in detail in section 2.4.2.

2.4.2 Adaptive surrogate-based optimization

The surrogate-based optimization algorithm requires to construct one surrogate over the whole design space. The global surrogate is then coupled to optimization algorithms. Surrogate model built with initial sampling dataset is usually not accurate enough to be applied in optimization problem. For this reason, various methods to update truth dataset have been explored. An effective method is to infill the optimal design of \hat{f} during last iteration with its truth response dataset. Given its advantage of low additional computational cost [Thelen, 2016], this infilling strategy is employed in this study. The main steps of the adaptive SBO algorithm are as follows:

1. Generate a group of initial sampling parameters using LHS method.
2. Apply the simulation models to obtain the truth response for all sampling parameters.
3. Choose proper approximation method (Gaussian Process, also known as Kriging model in this framework) to construct the surrogate model based on the sampling parameters with their truth response.
4. Couple surrogate model to the optimization algorithm and obtain optimum of the surrogate.
5. Check if maximum number of iteration is exceeded or optimal design converges. If not, repeat (2) - (4).

The workflow of this adaptive SBO method is illustrated in figure 4. As the optimization evolves, the adaptive samples with their truth response are infilled into the dataset and surrogate becomes increasingly accurate. Finally, the optimal solution is obtained.

Genetic algorithm (GA) is selected as the optimization algorithm in this study due to its wide application in WFLO problems as shown in table 1. The process of GA includes population initialization, selection of the most fitted individuals, application of some natural processes such as crossover and mutation, and population reproduction [Liu et al., 2021]. The detailed information of these steps is shown as follows:

1. Population initialization. Initialize a random population and then compute the value of the fitness function for each individual.

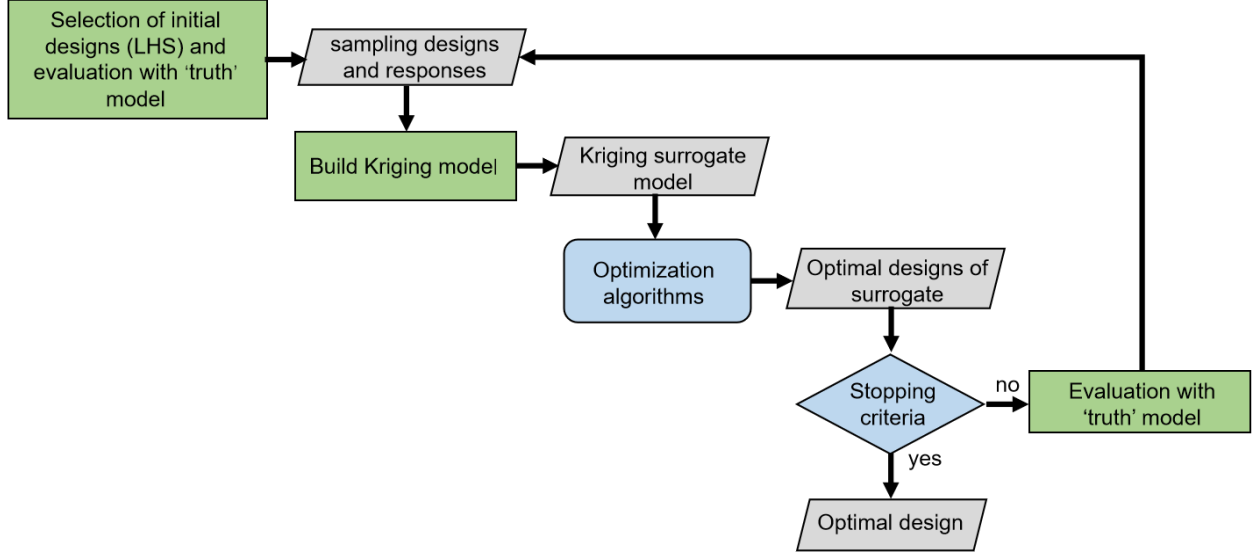


Figure 4: Workflow of the adaptive SBO method

Table 2: Settings for the self-adaptive framework.

| Parameters | Value |
|----------------------|-------|
| Initial dataset size | 360 |
| Population size | 50 |
| Crossover rate | 0.95 |
| Mutation rate | 0.15 |
| Maximum iterations | 1000 |

2. Selection. Individuals in population which do not satisfy constraints will be eliminated or multiplied by a penalty parameter. Then the algorithm selects suitable parents from individuals based on their fitness value. These parent individuals are further used for mating and generating new population.
3. Crossover and mutation. Randomly select two parent individuals. Then the process of crossover and mutation are performed according to crossover and mutation rate respectively. This step aims at creating offspring individuals and preventing GA from converging to local optimum solution.
4. Check convergence. If the convergence criteria is satisfied or maximum number of evaluations is exceeded, the iteration ends. Otherwise, repeat step II.

3 Case studies

In this section, three wind farm cases with different wind directions and terrains are studied using the self-adaptive optimization framework. As a reference, the more computationally expensive CFD-GA optimization (without surrogate model) is also carried out. The optimized results are then discussed and compared to the conventional staggered layout along the major wind direction (baseline) to assess the performance of the developed framework. The self-adaptive optimization framework settings for the three cases are summarized in table 2. Detailed case descriptions are presented in §3.1. Results and discussions are presented in §3.2.

3.1 Case descriptions

We use the NREL 5 MW reference turbine [Jonkman et al., 2009] as the wind turbine model in this study. The key parameters in the numerical modeling are listed in the table 3. The thrust and torque curves of the NREL 5 MW wind turbine as shown in figure 5 are inserted into the ADM code as mentioned in figure 4.

We optimize the layout of an 8-turbine wind farm within an $8D \times 8D$ rectangle, which is decomposed into 8×8 cells. The 81 nodes are prescribed as the potential positions for the eight turbines. We evaluate the performance of

Table 3: Key parameters of NREL 5 MW wind turbine

| Parameters | Value |
|------------------|----------|
| Diameter (D) | 126 m |
| Hub height | 90 m |
| Rated wind speed | 11.4 m/s |
| Rated power | 5 MW |
| Cut-in speed | 3 m/s |
| Cut-out speed | 25 m/s |

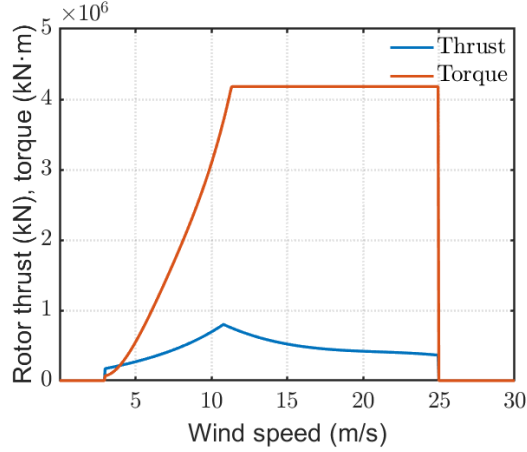


Figure 5: Thrust and torque curves for NREL 5 MW wind turbine

the proposed WFLO framework in three representative cases as shown in table 4. In Case I, only one wind direction with $U_\infty = 11.4$ m/s is considered. In Case II, a wind rose with eight wind directions (shown in figure 6) is taken into consideration. On this basis, case III further considers the effects of the terrain on the wind farm layout by the addition of an Gaussian-shaped hill with the height of 150 m on the bottom boundary.

3.2 Optimization results and discussion

The optimized and baseline layouts with their AEP distribution are shown in figure 7 to 9, and the number of CFD calls for different optimization strategies along with their AEPs are listed in table 5. Compared to baseline layouts, optimized layouts obtained from this framework and CFD-GA method both achieve significant AEP improvement. Due to the multi-modality of the WFLO problem, the optimization process can get stuck in a local minimum, thus the optimal layout results obtained from the CFD-GA and SBO strategies are usually not identical even for the same case. Nevertheless, the AEP of optimized layouts obtained from SBO are almost the same from that obtained by CFD-GA. In terms of computational cost, the numbers of CFD calls for SBO are 437, 400 and 399, compared to 961, 793 and 885 for CFD-GA in case I, case II and case III, respectively. These CFD simulations are executed on two desktop computers, both equipped with AMD EPYC 7532 processor with 32 cores. For the three wind farm cases, it takes approximately 72 h, 336 h and 360 h to obtain optimized layouts using CFD-GA method while it only takes approximately 36 h, 172 h and 190 h using the developed framework. Above all, we see that the surrogate-based optimization framework takes

Table 4: Definition for 3 WFLO cases

| | Case I | Case II | Case III |
|-----------------|----------------|----------------|----------------------|
| Turbine numbers | 8 | 8 | 8 |
| Restricted area | $8D \times 8D$ | $8D \times 8D$ | $8D \times 8D$ |
| Wind directions | 1 | 8 | 8 |
| Terrains | flat terrain | flat terrain | Gaussian-shaped hill |

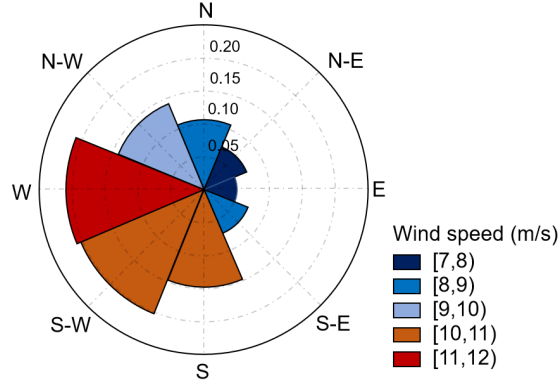


Figure 6: Wind rose for case II and case III

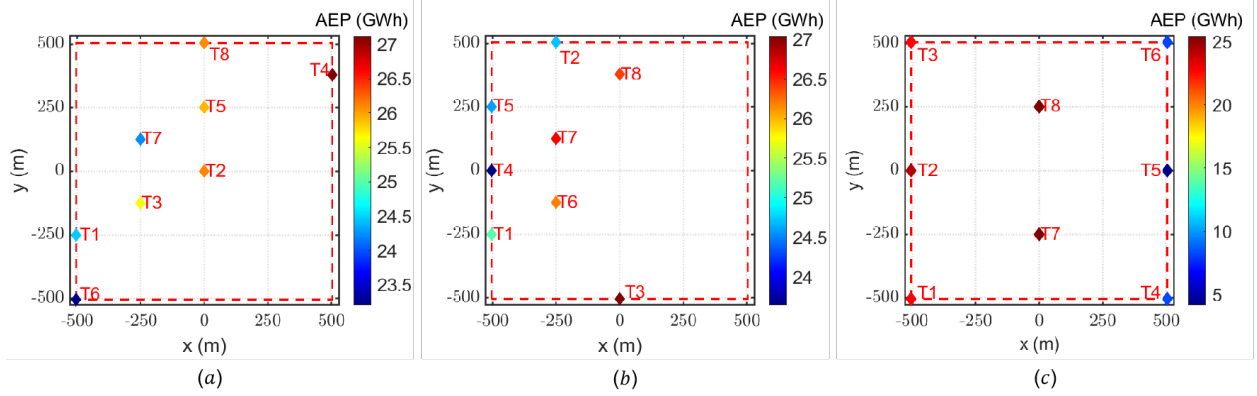


Figure 7: Case I: AEP distribution for layouts obtained from (a) SBO (b) CFD-GA and (c) baseline. The turbines are colored based on their individual AEPs.

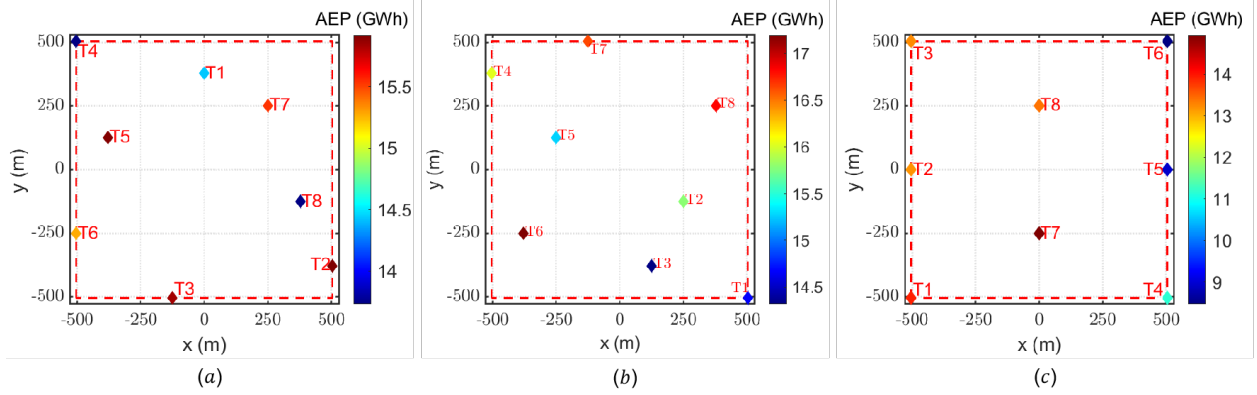


Figure 8: Case II: AEP distribution for layouts obtained from (a) SBO (b) CFD-GA and (c) baseline.

Table 5: AEP and CFD calls of optimized layouts using different optimization strategy for 3 cases

| | Case I | | Case II | | Case III | |
|----------|-----------|-----------|-----------|-----------|-----------|-----------|
| | CFD calls | AEP (GWh) | CFD calls | AEP (GWh) | CFD calls | AEP (GWh) |
| SBO | 437 | 202.740 | 400 | 120.374 | 399 | 178.037 |
| CFD-GA | 961 | 204.400 | 793 | 126.707 | 885 | 183.054 |
| Baseline | - | 141.324 | - | 97.287 | - | 135.732 |

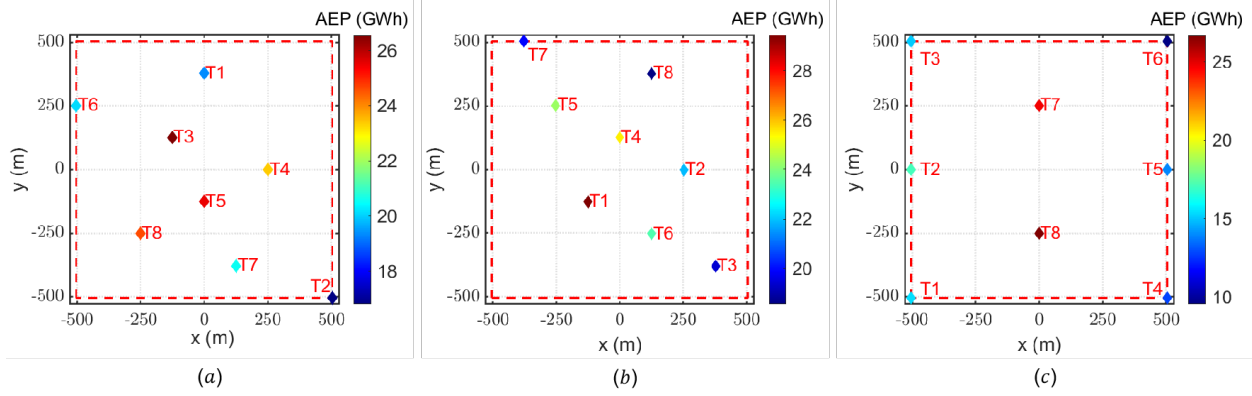


Figure 9: Case III: AEP distribution for layouts obtained from (a) SBO (b) CFD-GA and (c) baseline.

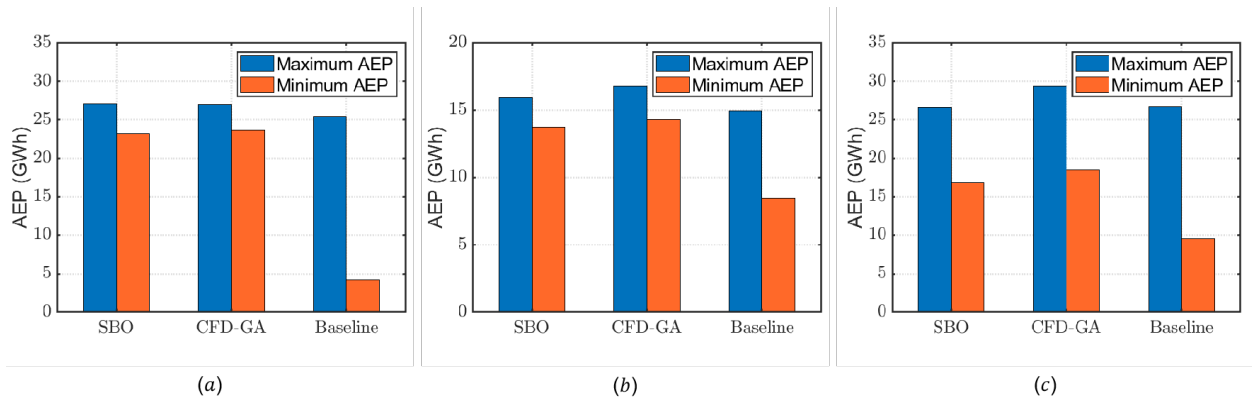


Figure 10: Comparison of maximum and minimum AEP of the turbines in the wind farm for optimal layouts for (a) Case I, (b) Case II, and (c) Case III.

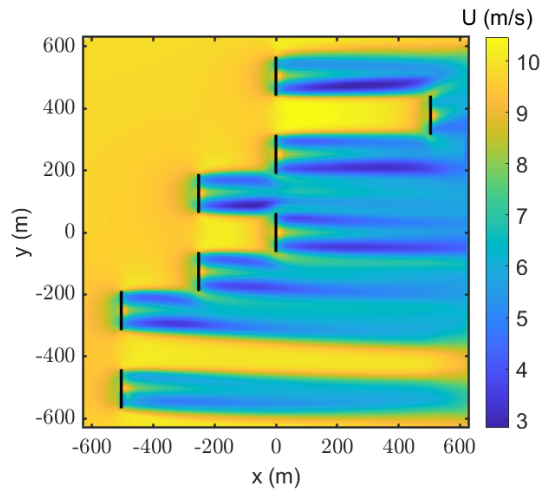


Figure 11: Velocity magnitude at rotor hub height of optimized layout for case I

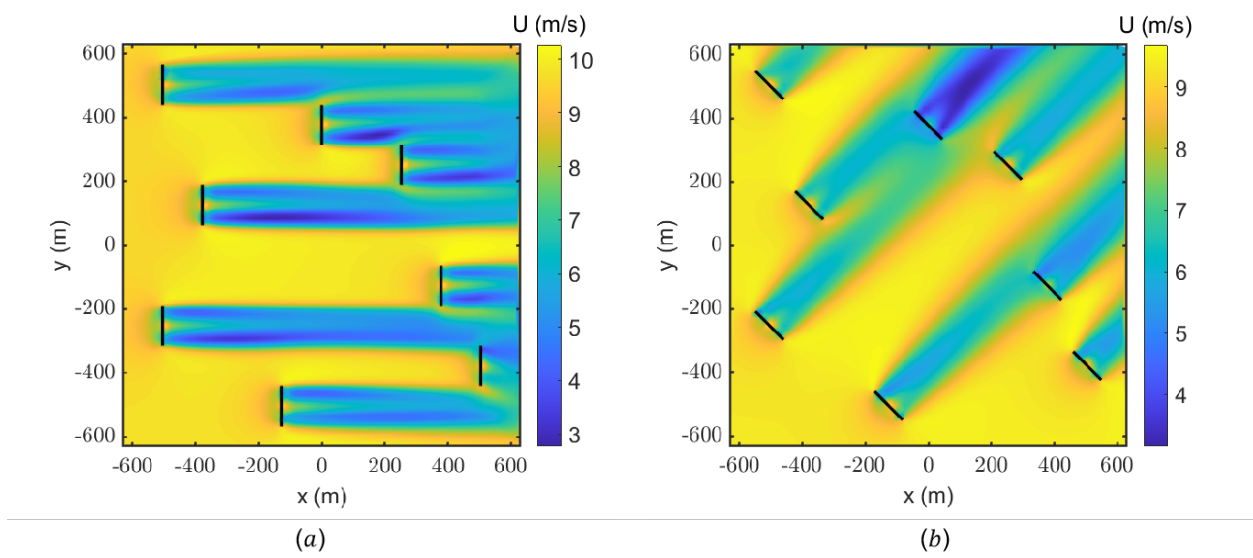


Figure 12: Velocity magnitude at rotor hub height of optimized layout for case II. (a) West, and (b) South-West.

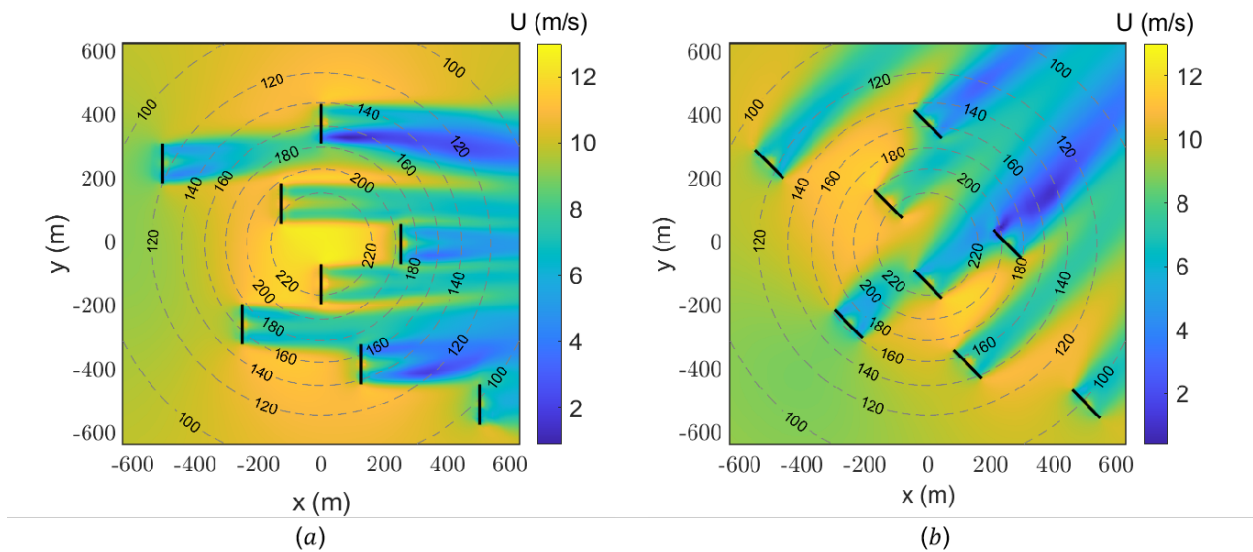


Figure 13: Velocity magnitude at rotor hub height of optimized layout for case III. (a) West, and (b) South-West. The gray dashed lines indicate the iso-height lines of the terrain.

only about half computational cost of the CFD-based method to find optimal designs which produce almost the same AEP.

We also compare the maximum and minimum AEP of the turbines in the wind farm for different layouts in figure 10. It is argued that, in a well-designed wind farm layout, the AEP among the different turbines should be distributed as even as possible, such that each turbine contribute a fair share to the total AEP. As shown in figure 10, the difference between maximum and minimum AEP in optimized layouts (obtained from both SBO and CFD-GA) is much smaller than that in baseline layouts for the two cases, indicating that AEP of optimized layouts becomes much more evenly-distributed. For case III, the difference between the maximum and minimum AEP is significantly larger. From figure 9, it is observed that the turbine associated with maximum AEP is located near the hill top, where the wind velocity increases due to the terrain effects. Nevertheless, the optimized layouts still feature more even AEP distribution than the reference layout.

We further show the velocity fields at the hub height of optimized layouts obtained from SBO in figures 11-13. For case I where only a single wind direction is considered, we notice that in SBO's optimized layout, all turbines are placed away from other turbines' wakes. In case II, the western inflow with wind speed of 11.3 m/s and occurrence frequency of 0.21 is the most dominant wind direction, and the southwestern inflow with wind speed of 10.9 m/s and occurrence frequency of 0.203 is the secondary dominant wind direction, as shown in the wind rose in figure 6. It is shown in figure 8 that most turbines are located away from other turbines' wake zone along the top two dominant wind directions. In case III, the effects of the terrain is considered. With the Gaussian hill at the center of the computational domain, the wind turbines in the optimized layouts are clustered toward the center to take advantage of the higher wind velocity. The ability of taking the terrain effects into consideration equips the current CFD-based WFLO method with more flexibility compared to those based on analytical wake models.

4 Conclusions

We have developed a surrogate-based framework for wind farm layout optimization with higher fidelity wake modeling methods, with the objective of maximizing the annual energy production. The surrogate is built by the Kriging model, which is trained using CFD simulations by treating the turbines as actuator disks. The surrogate model is then integrated with the genetic algorithm as the optimizer. During the optimization process, the wind farm layout dataset is updated adaptively with the intermediate design during each iteration added into it until the algorithm converges to the optimal layout. To assess its performance, we have tested the proposed SBO framework in three WFLO cases with different wind distributions and terrain. It is observed that the optimized layouts obtained from this self-adaptive framework generates almost similar AEP with CFD-GA direct optimization (without surrogate), and significantly outperforms the conventional staggered layout along the major wind direction. Aided by the surrogate modeling technique, the computational time of SBO framework is only half of that for the direct method, thus allowing the CFD-based WFLO to be carried out with manageable cost.

While the current study has demonstrated the feasibility of using Kriging model to accelerate high-fidelity wind farm layout optimization, there are still some limitations in the framework that need further improvement. First, the use of Gaussian process for building surrogate models is known to be "cursed" for high-dimensional data [Binois and Wycoff, 2022]. Innovative techniques for solving the scalability problem are in urgent need if this SBO framework is to be applied in WFLO tasks with larger number of wind turbines. Second, current work considers a single objective of maximizing AEP. Additional objectives, such as minimizing fatigue loads, minimizing construction cost, etc. can be incorporated in future studies. In addition, multi-fidelity methods have shown great potential in a variety of complex design problems [Forrester et al., 2007, Kou and Zhang, 2019, Jasa et al., 2022]. For WFLO, the results from low-fidelity analytical wake models can also be expected to play an important role in further improving the optimization efficiency using the multi-fidelity optimization framework.

Acknowledgments

DZ, ZH, KZ acknowledge financial support from the Innovation Program of Shanghai Municipal Education Commission (no. 2019-01-07-00-02-E00066), National Science Foundation of China (grant numbers: 12202271, 52122110, 42076210), Program for Intergovernmental International S&T Cooperation Projects of Shanghai Municipality, China (grant no. 22160710200), and the Oceanic Interdisciplinary Program of Shanghai Jiao Tong University (grant no. SL2020PT201).

References

- Rebecca Jane Barthelmie, K Hansen, Sten Tronæs Frandsen, Ole Rathmann, JG Schepers, W Schlez, J Phillips, K Rados, A Zervos, ESa Politis, et al. Modelling and measuring flow and wind turbine wakes in large wind farms offshore. *Wind Energy: An International Journal for Progress and Applications in Wind Power Conversion Technology*, 12(5): 431–444, 2009.
- Sohail R Reddy. Wind farm layout optimization (WindFLO): An advanced framework for fast wind farm analysis and optimization. *Applied Energy*, 269:115090, 2020.
- Hongyang Dong, Jincheng Zhang, and Xiaowei Zhao. Intelligent wind farm control via deep reinforcement learning and high-fidelity simulations. *Applied Energy*, 292:116928, 2021.
- Jared J Thomas, Nicholas F Baker, Paul Malisani, Erik Quaeghebeur, Sebastian Sanchez Perez-Moreno, John Jasa, Christopher Bay, Federico Tilli, David Bieniek, Nick Robinson, et al. A comparison of eight optimization methods applied to a wind farm layout optimization problem. *Wind Energy Science*, 8:865–891, 2022a.
- GPCDB Mosetti, Carlo Poloni, and Bruno Diviacco. Optimization of wind turbine positioning in large windfarms by means of a genetic algorithm. *Journal of Wind Engineering and Industrial Aerodynamics*, 51(1):105–116, 1994.
- U Aytun Ozturk and Bryan A Norman. Heuristic methods for wind energy conversion system positioning. *Electric Power Systems Research*, 70(3):179–185, 2004.
- SA Grady, MY Hussaini, and Makola M Abdullah. Placement of wind turbines using genetic algorithms. *Renewable Energy*, 30(2):259–270, 2005.
- Jose Castro Mora, Jose M Calero Baron, Jesus M Riquelme Santos, and Manuel Burgos Payan. An evolutive algorithm for wind farm optimal design. *Neurocomputing*, 70(16-18):2651–2658, 2007.
- Changshui Zhang, Guangdong Hou, and Jun Wang. A fast algorithm based on the submodular property for optimization of wind turbine positioning. *Renewable Energy*, 36(11):2951–2958, 2011.
- Yunus Eroğlu and Serap Ulusam Seçkiner. Design of wind farm layout using ant colony algorithm. *Renewable Energy*, 44:53–62, 2012.
- Ying Chen, Hua Li, Kai Jin, and Qing Song. Wind farm layout optimization using genetic algorithm with different hub height wind turbines. *Energy Conversion and Management*, 70:56–65, 2013.
- Jinkyoo Park and Kincho H Law. Layout optimization for maximizing wind farm power production using sequential convex programming. *Applied Energy*, 151:320–334, 2015.
- Rabia Shakoor, Mohammad Yusri Hassan, Abdur Raheem, and Nadia Rasheed. The modelling of wind farm layout optimization for the reduction of wake losses. *Indian Journal of Science and Technology*, 8(17):1–9, 2015.
- Peng Hou, Weihao Hu, Cong Chen, Mohsen Soltani, and Zhe Chen. Optimization of offshore wind farm layout in restricted zones. *Energy*, 113:487–496, 2016.
- Pieter Gebraad, Jared J Thomas, Andrew Ning, Paul Fleming, and Katherine Dykes. Maximization of the annual energy production of wind power plants by optimization of layout and yaw-based wake control. *Wind Energy*, 20(1):97–107, 2017.
- Leandro Parada, Carlos Herrera, Paulo Flores, and Victor Parada. Wind farm layout optimization using a gaussian-based wake model. *Renewable Energy*, 107:531–541, 2017.
- Ajit C Pillai, John Chick, Mahdi Khorasanchi, Sami Barbouchi, and Lars Johanning. Application of an offshore wind farm layout optimization methodology at middelgrunden wind farm. *Ocean Engineering*, 139:287–297, 2017.
- Nicolas Kirchner-Bossi and Fernando Porté-Agel. Realistic wind farm layout optimization through genetic algorithms using a Gaussian wake model. *Energies*, 11(12):3268, 2018.
- Andrew PJ Stanley and Andrew Ning. Massive simplification of the wind farm layout optimization problem. *Wind Energy Science*, 4(4):663–676, 2019.
- Ning Quan and Harrison M Kim. Greedy robust wind farm layout optimization with feasibility guarantee. *Engineering Optimization*, 51(7):1152–1167, 2019.
- Luís Eduardo Boni Cruz and Bruno Souza Carmo. Wind farm layout optimization based on CFD simulations. *Journal of the Brazilian Society of Mechanical Sciences and Engineering*, 42:1–18, 2020.
- Enrico GA Antonini, David A Romero, and Cristina H Amon. Optimal design of wind farms in complex terrains using computational fluid dynamics and adjoint methods. *Applied Energy*, 261:114426, 2020.
- Andrew PJ Stanley, Jennifer King, and Andrew Ning. Wind farm layout optimization with loads considerations. In *Journal of Physics: Conference Series*, volume 1452, page 012072. IOP Publishing, 2020.

- Bertelsen Gagakuma, Andrew PJ Stanley, and Andrew Ning. Reducing wind farm power variance from wind direction using wind farm layout optimization. *Wind Engineering*, 45(6):1517–1530, 2021.
- Zhenqing Liu, Shuanglong Fan, Yize Wang, and Jie Peng. Genetic-algorithm-based layout optimization of an offshore wind farm under real seabed terrain encountering an engineering cost model. *Energy Conversion and Management*, 245:114610, 2021.
- Jared J Thomas, Spencer McOmber, and Andrew Ning. Wake expansion continuation: Multi-modality reduction in the wind farm layout optimization problem. *Wind Energy*, 25(4):678–699, 2022b.
- Niels Otto Jensen. *A note on wind generator interaction*. Report Risø-M-2411, Risø National Laboratory, Roskilde, Denmark, 1983.
- Gunner Chr Larsen. *A simple wake calculation procedure*. Report Riso-M-2760, Risø National Laboratory, Roskilde, Denmark, 1988.
- Sten Frandsen, Rebecca Barthelmie, Sara Pryor, Ole Rathmann, Søren Larsen, Jørgen Højstrup, and Morten Thøgersen. Analytical modelling of wind speed deficit in large offshore wind farms. *Wind Energy: An International Journal for Progress and Applications in Wind Power Conversion Technology*, 9(1-2):39–53, 2006.
- Anshul Mittal, Kidambi Sreenivas, Lafayette K Taylor, Levi Hereth, and Christopher B Hilbert. Blade-resolved simulations of a model wind turbine: effect of temporal convergence. *Wind Energy*, 19(10):1761–1783, 2016.
- Yuanchuan Liu, Qing Xiao, Atilla Incecik, Christophe Peyrard, and Decheng Wan. Establishing a fully coupled CFD analysis tool for floating offshore wind turbines. *Renewable Energy*, 112:280–301, 2017.
- Marielle de Oliveira, Rodolfo Curci Puraca, and Bruno Souza Carmo. Blade-resolved numerical simulations of the nrel offshore 5 mw baseline wind turbine in full scale: A study of proper solver configuration and discretization strategies. *Energy*, 254:124368, 2022.
- Zhihao Zhang, Limin Kuang, Zhaolong Han, Dai Zhou, Yongsheng Zhao, Yan Bao, Lei Duan, Jiahuang Tu, Yaoran Chen, and Mingsheng Chen. Comparative analysis of bent and basic winglets on performance improvement of horizontal axis wind turbines. *Energy*, 281:128252, 2023.
- Richard J. A. M. Stevens and Charles Meneveau. Flow structure and turbulence in wind farms. *Annual Review of Fluid Mechanics*, 49:311–339, 2017.
- Richard J. A. M. Stevens, Luis A Martínez-Tossas, and Charles Meneveau. Comparison of wind farm large eddy simulations using actuator disk and actuator line models with wind tunnel experiments. *Renewable Energy*, 116:470–478, 2018.
- Carl R Shapiro, Genevieve M Starke, and Dennice F Gayme. Turbulence and control of wind farms. *Annual Review of Control, Robotics, and Autonomous Systems*, 5:579–602, 2022.
- Benjamin Sanderse, SP Van der Pijl, and Barry Koren. Review of computational fluid dynamics for wind turbine wake aerodynamics. *Wind Energy*, 14(7):799–819, 2011.
- Erik Svenning. Implementation of an actuator disk in openfoam. *Chalmers University of Technology*, 2010.
- Luis A Martínez-Tossas, Matthew J Churchfield, and Stefano Leonardi. Large eddy simulations of the flow past wind turbines: actuator line and disk modeling. *Wind Energy*, 18(6):1047–1060, 2015.
- Daniel G Krige. *A statistical approach to some mine valuation and allied problems on the Witwatersrand*. PhD thesis, University of the Witwatersrand, 1951.
- Jason W Karl. Spatial predictions of cover attributes of rangeland ecosystems using regression kriging and remote sensing. *Rangeland Ecology & Management*, 63(3):335–349, 2010.
- S G Casella. Surrogate based optimisation for hull shapes with dakota toolkit. Master’s thesis, Delft University of Technology, 2020.
- M Cid Montoya, S Hernández, and Ahsan Kareem. Aero-structural optimization-based tailoring of bridge deck geometry. *Engineering Structures*, 270:114067, 2022.
- Fangyun Bai, Xinglong Ju, Shouyi Wang, Wenyong Zhou, and Feng Liu. Wind farm layout optimization using adaptive evolutionary algorithm with Monte Carlo Tree Search reinforcement learning. *Energy Conversion and Management*, 252:115047, 2022.
- Michael D McKay, Richard J Beckman, and William J Conover. A comparison of three methods for selecting values of input variables in the analysis of output from a computer code. *Technometrics*, 42(1):55–61, 2000.
- Mark Richmond, A Antoniadis, Lin Wang, Athanasios Kolios, S Al-Sanad, and Jafarali Parol. Evaluation of an offshore wind farm computational fluid dynamics model against operational site data. *Ocean Engineering*, 193:106579, 2019.

- Tony Burton, Nick Jenkins, David Sharpe, and Ervin Bossanyi. *Wind energy handbook*. John Wiley & Sons, 2011.
- Sydney Goldstein. On the vortex theory of screw propellers. *Proceedings of the Royal Society of London. Series A, Containing Papers of a Mathematical and Physical Character*, 123(792):440–465, 1929.
- Keith Dalbey, Michael Eldred, Gianluca Geraci, John Jakeman, Kathryn Maupin, Jason A Monschke, Daniel Seidl, Anh Tran, Friedrich Menhorn, and Xiaoshu Zeng. Dakota, a multilevel parallel object-oriented framework for design optimization, parameter estimation, uncertainty quantification, and sensitivity analysis: Version 6.16 theory manual. Technical report, Sandia National Lab.(SNL-NM), Albuquerque, NM (United States), 2022.
- Brian M Adams, William J Bohnhoff, Keith R Dalbey, Mohamed S Ebeida, John P Eddy, Michael S Eldred, Russell W Hooper, Patricia D Hough, Kenneth T Hu, John D Jakeman, et al. Dakota, a multilevel parallel object-oriented framework for design optimization, parameter estimation, uncertainty quantification, and sensitivity analysis: version 6.13 user’s manual. Technical report, Sandia National Lab.(SNL-NM), Albuquerque, NM (United States), 2020.
- Andrew Thelen. *Surrogate-based design optimization of dual-rotor wind turbines using steady RANS equations*. PhD thesis, Iowa State University, 2016.
- Jason Jonkman, Sandy Butterfield, Walter Musial, and George Scott. Definition of a 5-MW reference wind turbine for offshore system development. Technical report, National Renewable Energy Lab.(NREL), Golden, CO (United States), 2009.
- Mickael Binois and Nathan Wycoff. A survey on high-dimensional gaussian process modeling with application to bayesian optimization. *ACM Transactions on Evolutionary Learning and Optimization*, 2(2):1–26, 2022.
- Alexander IJ Forrester, András Sóbester, and Andy J Keane. Multi-fidelity optimization via surrogate modelling. *Proceedings of the Royal Society A: Mathematical, Physical and Engineering Sciences*, 463(2088):3251–3269, 2007.
- Jiaqing Kou and Weiwei Zhang. Multi-fidelity modeling framework for nonlinear unsteady aerodynamics of airfoils. *Applied Mathematical Modelling*, 76:832–855, 2019.
- John Jasa, Pietro Bortolotti, Daniel Zalkind, and Garrett Barter. Effectively using multifidelity optimization for wind turbine design. *Wind Energy Science*, 7(3):991–1006, 2022.